



Physical and micro-structural characteristics of limestone after high temperature exposure

Qing-Bin Meng¹ · Cong-Kai Wang¹ · Jiang-Feng Liu¹ · Ming-Wei Zhang¹ · Meng-Meng Lu¹ · Yu Wu¹

Received: 30 November 2018 / Accepted: 24 September 2019 / Published online: 31 October 2019
© Springer-Verlag GmbH Germany, part of Springer Nature 2019

Abstract

Temperature is a major factor affecting physical and mechanical rock properties. With increasing temperature, a series of variations enlarge the internal defects within rocks, resulting in physical and mechanical rock property variations. To explore the influence of temperature on the physical and micro-structure of limestone, the weighing test and *P*-wave velocity test were conducted on limestone after exposure to high temperature to reveal the evolution of the limestone mass and *P*-wave velocity. XRD, XRF, SEM, and mercury intrusion tests were also carried out to examine the mineral composition and content, micro-fracture morphology, porosity, and fractal dimension. The limestone mass and *P*-wave velocity decrease with increasing temperature. When $T \leq 400$ °C, there is no obvious change in chemical composition and crystal structure; when $T = 400$ – 500 °C, the diffraction intensity of partial calcite decreases, and dolomite decomposes gradually; when $T > 500$ °C, illite decomposes gradually, while dolomite decomposes completely; and the diffraction intensity of calcite is significantly reduced. When $T \leq 200$ °C, changes in trace minerals or impurities containing K_2O and Na_2O and the decomposition of illite oxide are dominant; when $T = 400$ – 600 °C, illite oxide, trace minerals, or impurities containing K_2O and calcium hydroxide begin to decompose. When $T = 600$ – 800 °C, magnesite and dolomite begin to decompose. When $T \leq 200$ °C, micro-fracture surfaces change slightly. When $T = 200$ – 500 °C, micro-fractures begin to develop and propagate gradually, most of which are intergranular cracks with a small number of transgranular cracks. When $T > 500$ °C, transgranular cracks occur in samples with locally broken crystals, and the cracking of the crystal structure occurs with increasing pore size. With increasing temperature, the limestone pore fractal dimension decreases gradually, and the higher the temperature, the greater the decrease. 400 °C to 500 °C is the temperature threshold interval that causes the pore structure change. These new pores, resulting from the increasing temperature, are primarily mesopores with a pore diameter of 1.0 – 10.0 μm . This research provides a scientific basis for the design and construction of rock engineering projects to be subjected to high temperatures, deep geological radioactive nuclear waste disposal sites, deep mines, and the exploitation of geothermal resources.

Keywords High-temperature rock · Micro-structure test · Mass and *P*-wave velocity · Mineral component and composition · Fractal dimension of porosity

Highlights

- The weighing test, *P*-wave velocity test, XRD test, XRF test, SEM test, and mercury intrusion test are conducted on limestone samples after exposure to high temperature (20 – 800 °C), revealing the physical and micro-structure evolution of limestone.
- With increasing temperature, mineral dilatancy, water loss, decomposition, phase transition of mineral components, and the breakage of chemical bonds result in increasing internal defects, leading to changes in physical and mechanical rock properties.
- With increasing temperature, the original microvoids and micro-fractures in the limestone gradually expand, and intergranular cracks generated in the samples at low temperature gradually change to intergranular cracks and transgranular cracks at high temperature.
- Limestone porosity increases gradually with increasing temperature. $T = 400$ – 500 °C can be used as a threshold interval for the change in limestone fractal dimension and mineral phase transition.

✉ Jiang-Feng Liu
jeaflu@hotmail.com

¹ State Key Laboratory for Geomechanics and Deep Underground Engineering, School of Mechanics and Civil Engineering, China University of Mining and Technology, Xuzhou 221116, China

Introduction

Physical and mechanical rock properties as well as rock deformation and failure characteristics after exposure to high temperatures are becoming increasingly important issues in modern rock engineering projects (Heuze 1983; David et al. 1999; Leiss and Molli 2003; Zhang et al. 2001a, b; Ranjith et al. 2012; Yang et al. 2014; Sun et al. 2016). Underground coal gasification mining, burial of high-level radioactive nuclear waste, utilization of deep underground space and geothermal resources, marine deep well drilling, as well as assessment and restoration of tunnels or buildings after a fire require an understanding of how high temperatures affect various rock types. Therefore, it is of great theoretical and practical significance to determine the effect of high temperatures on rock physical and mechanical properties.

The study of physical and mechanical rock properties at high temperature is a relatively a new field in rock mechanics. The evolution of rock strength and deformation parameters are obtained in certain researches (Rocchi et al. 2004; Zhang et al. 2009; Lu et al. 2017; Ersoy et al. 2019). Alm et al. (1985) investigated mechanical properties of granite subjected to different heating treatments and discussed the fracturing process of granite under various temperatures. Su et al. (2015) examined the basic mechanical properties (elastic modulus, Poisson's ratio, uniaxial compressive strength, and peak strain) of red sandstone after exposure to 200–800 °C temperatures, and determined how strength and deformation parameters vary with temperature. Chen et al. (2012) investigated mechanical properties of granite under high temperature using uniaxial tests. With increasing temperature, the peak stress and elastic modulus of granite gradually decreased, while the peak strain gradually increased. The amount of change is small below 400 °C but increases rapidly above 400 °C. Brotóns et al. (2013) analyzed the effect of temperature on the mechanical properties of carbonate rocks. The uniaxial compressive strength, elasticity modulus, and Poisson's ratio gradually decreased with increasing temperature between 105 and 600 °C. Wu et al. (2013) conducted an experimental study on the mechanical properties of sandstone under temperatures ranging from 20 to 1200 °C. The peak stress and elastic modulus of sandstone decreased gradually with increasing temperature. Heard (1980) analyzed the thermal dilatation coefficient and permeability of rocks and showed that the rock thermal dilatation coefficient increases with increasing temperature. Zhang et al. (2001a) conducted an experimental study on the connectivity and permeability of marble under high temperature, and showed that the permeability of marble is increased significantly between 327 and 427 °C. Lo and Wai (1982) studied the variation of thermal diffusivity of limestone and gneiss after high temperature

treatment. Results showed that the thermal diffusivity of limestone and gneiss decreased with increasing temperature. Molen (1981) discussed the temperature effect of quartz phase transitions on the thermal dilatation coefficient, and determined the temperature range of quartz's phase transition. Using X-ray diffraction, microprobe analysis, and chemical analysis, Just and Kontny (2012) analyzed granite mineral compositions under high temperature. Hajpál (2002) heated German and Hungarian sandstones from 150 to 900 °C and recorded the changes in mineral composition, porosity, density, fractures, and ultrasonic velocity of sandstones before and after high temperature treatment using X-ray diffraction (XRD), scanning electron microscopy (SEM), and ultrasonic detection. Yavuz et al. (2010) considered the effect of high temperature on the physical properties of marble and limestone and analyzed the variation of grain size, porosity, and structural characteristics with temperature. Ferrero and Marini (2001) examined marble at temperatures ranging from 230 to 600 °C, obtained the density of marble at different temperatures, and analyzed the influence of density variations on rock mechanical behaviors. Sun et al. (2015) carried out physical and microscopic experiments on granite after high temperature treatment at 25–800 °C and analyzed the influence of temperature on the physical properties of granite. Yang et al. (2017) observed high-temperature treated granite under an optical microscope and determined that the size of the thermal crack on the granite surface increased with increasing temperature. Zhang and Sun (2018) performed high temperature tests on limestone at 25–800 °C and quantitatively studied the variation of mineral elements using X-ray fluorescence (XRF). Tian et al. (2012) studied physical properties of sandstone after exposure to high temperature and concluded that sandstone density decreased significantly after 500 °C, and porosity increased significantly after 300 °C. Sandstone permeability increased gradually with increasing temperature.

In summary, studies on the effect of temperature on physical and mechanical rock properties are numerous; however, these studies mainly concentrate on macroscopic temperature effects, such as rock strength and deformation parameters, while studies on rock microstructure at high-temperatures are rare. Thermal stress results in thermal fracturing of rock and causes other physical changes (density, wave velocity, mineral composition, mineral element content, fracture morphology, and pore structure) and affects macroscopic mechanical rock parameters. Therefore, it is necessary to study the effect of temperature on the physical and microscopic parameters of rocks in order to provide a scientific basis for the design and construction of high-temperature rock engineering projects.

Experimental testing scheme for limestone subjected to high temperatures

Limestone samples were collected from Xuzhou, Jiangsu Province, China. The limestone is gray with an average density of $2.71\text{--}2.73\text{ g/cm}^3$, has an overall uniform texture, and is primarily composed of calcite, dolomite, and illite. Rock samples are processed into cylinders 50 mm in diameter and

100 mm in height. GWD-02A Annealing Furnaces, developed by the Ceramics Research Institute of Light Industry of China, are used to heat rock samples (Fig. 1a). Samples are heated to 20 °C, 200 °C, 400 °C, 500 °C, 600 °C, and 800 °C at a rate of 10 °C/min. After reaching the specified temperature, the temperature is held constant for 4 h to ensure a uniform heat distribution inside the sample (Heap et al. 2009; Ranjith et al. 2012; Su et al. 2017; Meng et al. 2019). Finally, the

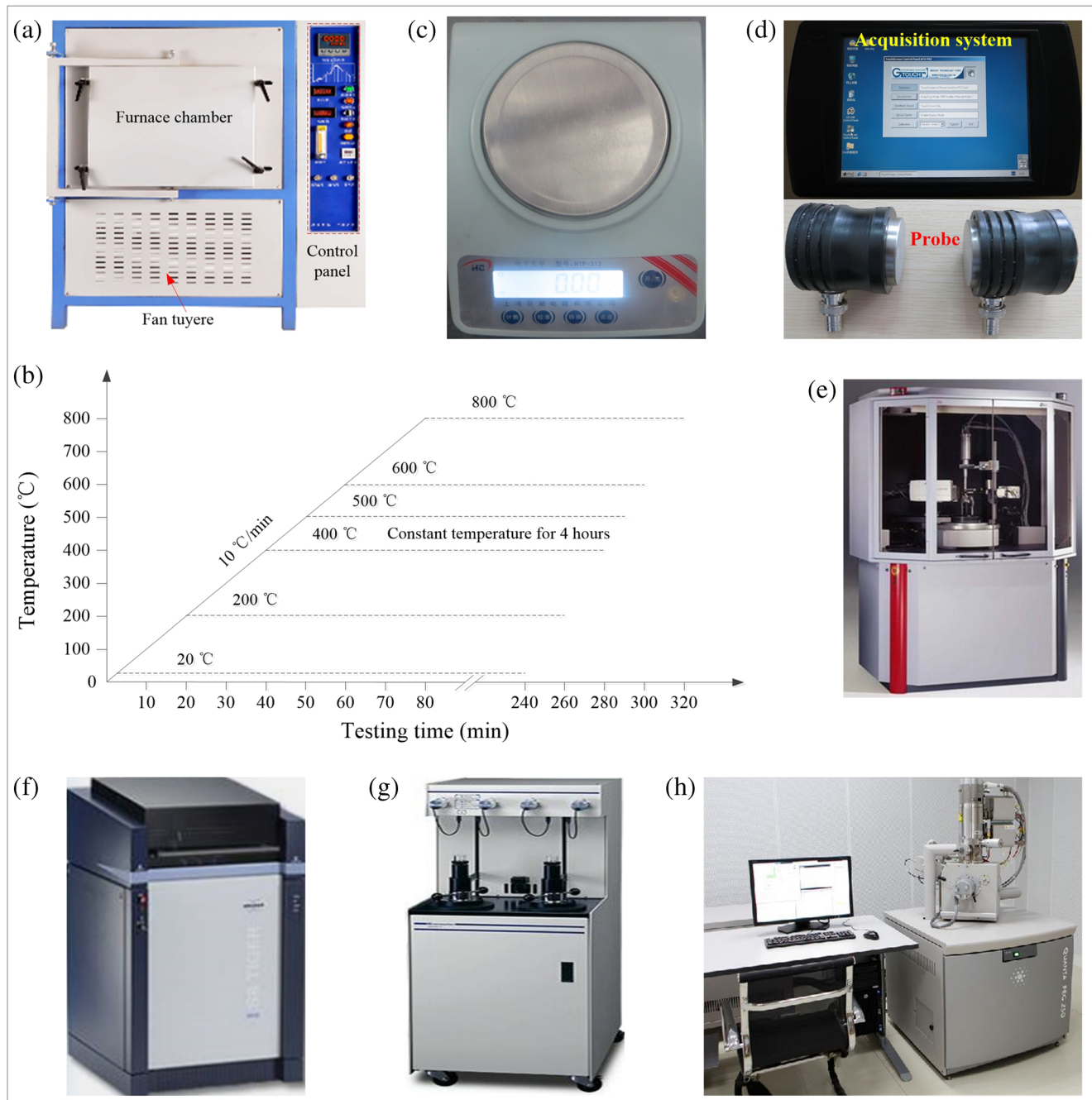


Fig. 1 Test heating curve and test equipment

sample is naturally cooled to room temperature, and the heating curve is shown in Fig. 1b. Eighteen rock samples were produced at each temperature for a total of 108 rock samples.

To understand the effect of high temperature on limestone physical and micro-structural properties, five types of tests are systematically conducted: (1) Samples were weighed after heating using HTP-312 high-precision electronic balance, manufactured by Shanghai Hochice Electrical Appliance Co., Ltd. (Fig. 1c). The electronic balance has a measurement range of 1000 g with an accuracy of 0.01 g. (2) Wave velocity tests were conducted using a RSM-SY6 Sonic Wave Detector (Fig. 1d) manufactured by Wuhan Sinorock Technology Co., Ltd. The sampling time is 0.1–200 μ s, and the sampling length is 0.5–1.0K bps. Prior to the test, Vaseline is applied to the upper and lower end faces of the rock sample as a coupling agent. (3) X-ray diffraction tests (XRD test) and X-ray fluorescence tests (XRF test) were carried out using a D8 Advance X-ray diffractometer (Fig. 1e) and S8 Tiger X-ray fluorescence spectrometer (Fig. 1f) produced by the Bruker Company in Germany. Before testing, rock samples are crushed to less than 200 meshes (74 μ m) and dried at 105 °C for more than 2 h in a drying oven. The sample weight is approximately 5–10 g. (4) Micro-fracture morphology tests were conducted using a FEI Quanta™ 250 scanning electron microscope produced by the FEI company in America (Fig. 1h). The selected magnifications are \times 500, \times 1000, \times 1500, \times 2000, \times 3000, and \times 5000. The resolution of this instrument is less than 3.5 nm, and the magnification is between 6 and 1 million times. Before the test, dust is removed from the surface of the rock sample, and a 5–10 nm thick layer of conductive metal is sprayed on the surface of the rock sample. (5) Mercury infusion tests are used to study the pore structure of limestone after exposure to high temperatures. A Model 9310 Microporous Structure Analyzer, which is manufactured by Micromeritics Instrument Co., Ltd., USA, is used to measure to pore structure (Fig. 1g) and has a measurement range of 0.006–360 μ m, a maximum working pressure of 207 MPa, and a resolution of 0.1 mm³. During the test, the rock samples are first dried in an oven at 105 °C to reach a constant weight (the mass of the rock samples remained unchanged for more than 7 d consecutively), then the rock samples were placed in a 6.67 Pa vacuum and injected with mercury. With increasing injection pressure (capillary pressure), mercury can enter pores of various sizes in the rock sample. During the test, the mercury pressure and cumulative mercury volume are automatically recorded. The injected mercury volume is determined by the variation of the platinum resistance wire exposing the mercury surface. The porosity of the rock sample and the proportion of pores of different diameters can be determined according to the volume of mercury entering the rock sample under different pressures.

Analysis of test results

Limestone mass loss after high temperature exposure

Under high temperature, the moisture inside the rock samples evaporates, and some minerals undergo decomposition and phase transformation. Dehydroxylation, namely the removal of hydroxyl groups (–OH) from organic compound molecules, and other physical and chemical reactions alter the mass of the sample. According to Eq. (1), the mass loss rate of limestone at different temperatures can be calculated. Specific values are shown in Table 1.

$$k_m = \frac{m_0 - m_1}{m_0} \times 100\% \quad (1)$$

where k_m is the mass loss rate, %; m_0 is the mass (average mass) of limestone sample before exposure to high temperature, kg; m_1 is the average mass of limestone sample after exposure to high temperature, kg.

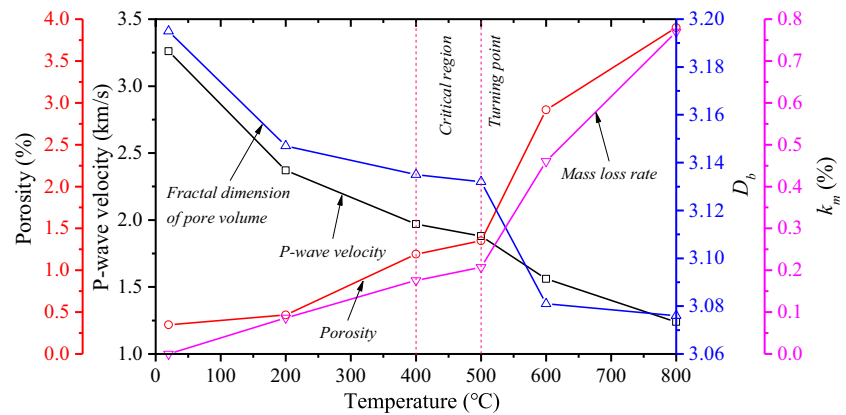
The mass loss rate of limestone increases gradually with increasing temperature, but the variation characteristics are different at different temperatures (Fig. 2 and Table 1). When $T < 400$ °C, the relative limestone mass reduction after exposure to high temperature is not obvious, and the mass loss rate is 0.18%. When $T = 400$ –500 °C, the mass variation is obvious, and the mass loss rate is 0.21%. When $T > 500$ °C, the mass loss rate increases sharply. When the temperature reaches 800 °C, the limestone mass loss rate is 0.77%, which is 3.67 times that at $T = 500$ °C. Evaporation of water inside the limestone, variation of certain mineral components, and the loss of structural water are main reasons for mass loss. Results show that the physical state of water inside the rock changes during the heating process (Sun et al. 2015; Zhang and Sun 2018). Attached water, bound water (strongly bound

Table 1 Limestone mass and *P*-wave velocity after high temperature exposure

Temperature (°C)	Average mass before high temperature action (kg)	Average mass after high temperature action (kg)	<i>P</i> -wave velocity before the high temperature (m/s)	<i>P</i> -wave velocity after high temperature (m/s)
20	534.40	/	3260.44	/
200	533.44	532.98	3260.39	2370.56
400	535.36	534.42	3260.50	1972.61
500	536.45	535.34	3260.44	1877.28
600	535.48	533.02	3260.39	1556.50
800	533.92	529.81	3260.56	1243.39

The data in the table is the average value of eighteen rock specimens

Fig. 2 Physical property variation of limestone with temperature



water, weak bound water), and mineral bound water (constitution water, crystalline water) vaporize and escape at different temperatures. Attached water escapes at $T = 100$ °C, strong bound water escapes at $T = 200$ – 300 °C, crystalline water escapes at $T = 300$ – 400 °C, and mineral bound water escapes at $T = 400$ – 500 °C. The loss of constitution water and crystalline water leads to the destruction of the lattice frame of minerals. The limestone mass loss is primarily caused by water loss inside the rock when $T < 500$ °C, resulting in a small variation in limestone mass loss rate. When $T \geq 500$ °C, minerals contained in the limestone gradually decompose. Magnesite (MgCO_3) is gradually decomposed into MgO and CO_2 . MgCO_3 decomposition is accelerated especially at $T = 500$ – 600 °C. Dolomite ($\text{CaMg}(\text{CO}_3)_2$) gradually decomposes into CaCO_3 and MgCO_3 at $T = 700$ – 800 °C and then decomposed into MgO and CO_2 , resulting in a sharp increase in mass loss rate between $T = 500$ and 800 °C.

P-wave velocity of limestone after high temperature exposure

P-wave velocity is an important parameter for rock mass evaluation (Kılıç 2006). After high temperature exposure, physical and chemical reactions, including dehydration, phase transition, chemical bond fracture, crack generation and expansion, and mineral expansion inside the rock lead to changes in the P-wave velocity (Fig. 2). Limestone P-wave velocity decreases with the increasing temperature. Based on P-wave velocity variations at different temperatures, the temperature range of 20–800 °C can be divided into three stages: (1) When $T = 20$ – 400 °C, P-wave velocity slowly decreases. The magnitude of the P-wave speed reduction is 27.29–39.50%. With increasing temperature, the generation of new cracks and the expansion of primary cracks results in a decreasing P-wave velocity. In addition, the gradual loss of internal attached water and mineral bound water and the phase transition and decomposition of some minerals lead to increased porosity and

internal damage, which decreases P-wave velocity. (2) When $T = 400$ – 500 °C, P-wave velocity slowly decreases by 39.50–42.42%. (3) When $T = 500$ – 800 °C, P-wave velocity decreases sharply by 42.42–61.87%. The change in P-wave velocity at this stage results in partial mineral decomposition and phase transition.

Mineral composition and elemental composition of limestone after high temperature exposure

X-ray diffraction (XRD) is a basic method of determining rock composition (Zhang et al. 2014). XRD tests were carried out for the limestone samples after high temperature exposure using a D8 Advance X-ray diffractometer. The diffraction results are given in Table 2. The X-ray diffraction pattern of the limestone rock samples at different temperatures is shown in Fig. 3. XRF tests on limestone sample after high temperature exposure were carried out using a S8 Tiger X-ray fluorescence spectrometer for limestone sample subjected to temperatures from 20 to 800 °C (Table 3). The variation of mineral composition with temperature is shown in Fig. 4.

Limestone diffraction patterns are similar when $T < 400$ °C (Fig. 3 and Table 2). The main mineral composition, diffraction angle, and diffraction intensity are relatively similar, indicating that the limestone chemical composition and crystal

Table 2 Mineral species and contents of limestone after high temperature exposure (%)

Temperature (°C)	Calcite	Dolomite	Illite
20	93.1	2.4	4.5
200	95.2	1.7	3.1
400	96.1	1.4	2.5
500	97.5	0.7	1.8
600	98.3	/	1.7
800	98.5	/	1.5

The data in the table is the average value of three rock specimens

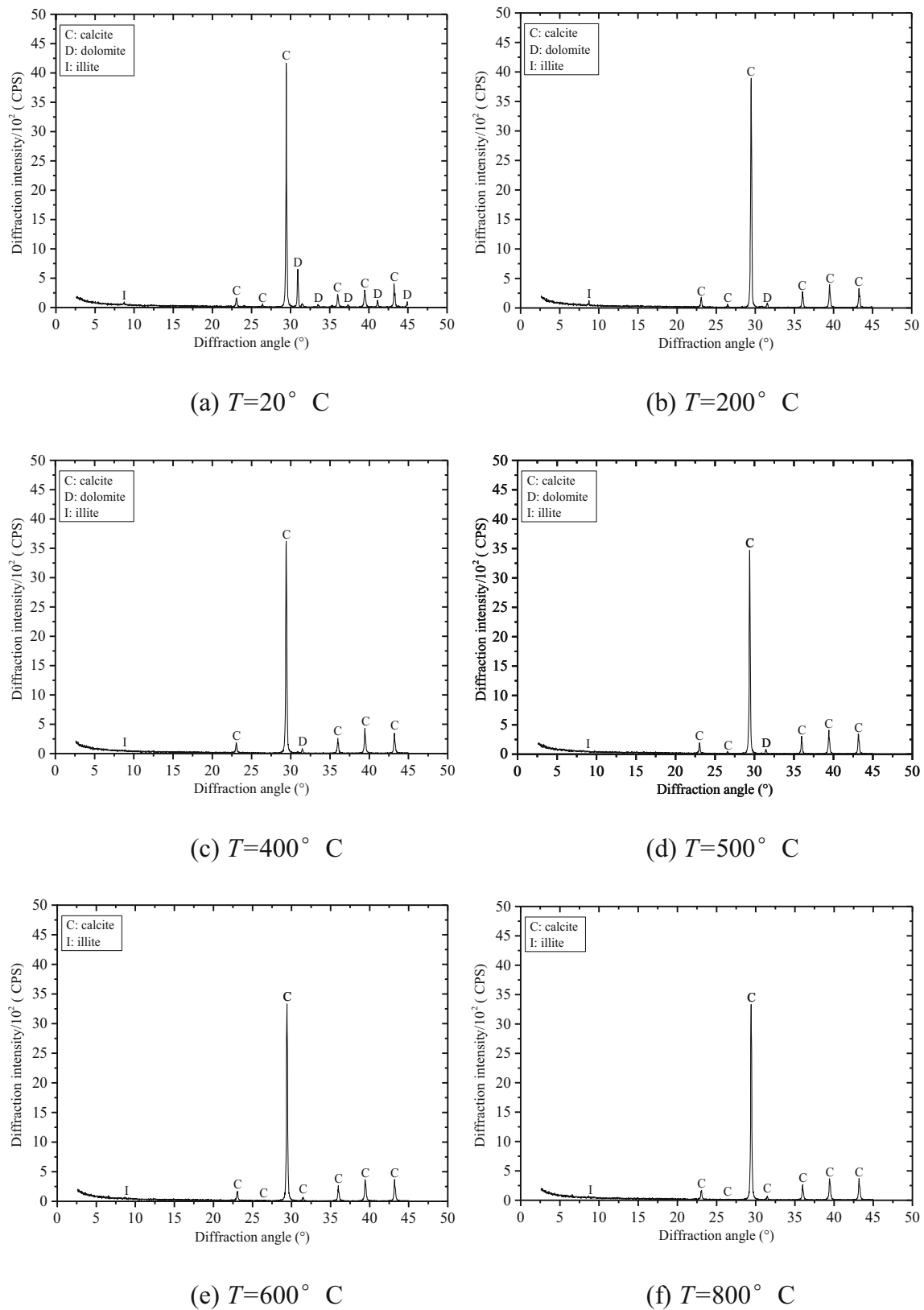


Fig. 3 X-ray diffraction patterns of limestone samples at different temperatures

structure are not changed significantly. When $T=400\text{--}500^{\circ}\text{C}$, the primary mineral components (illite) of limestone

remains unchanged; the diffraction intensity of some calcite is decreased, and dolomite is decomposed gradually. When $T>$

Table 3 Mineral compositions and contents of limestone after high temperature exposure (%)

Mineral elements	Temperature (°C)					
	20	200	400	500	600	800
Na ₂ O	0.301	0.277	0.154	0.087	0.067	0.052
MgO	1.874	1.642	1.482	1.114	1.699	2.076
Al ₂ O ₃	3.305	2.775	2.375	1.522	1.952	2.515
SiO ₂	10.754	9.683	8.761	7.835	8.724	9.121
K ₂ O	0.169	0.138	0.116	0.102	0.124	0.158
CaO	48.187	48.643	49.194	49.823	48.348	48.762
Fe ₂ O ₃	0.242	0.212	0.118	0.107	0.167	0.254
CO ₂	35.168	36.630	37.800	39.410	38.919	37.062

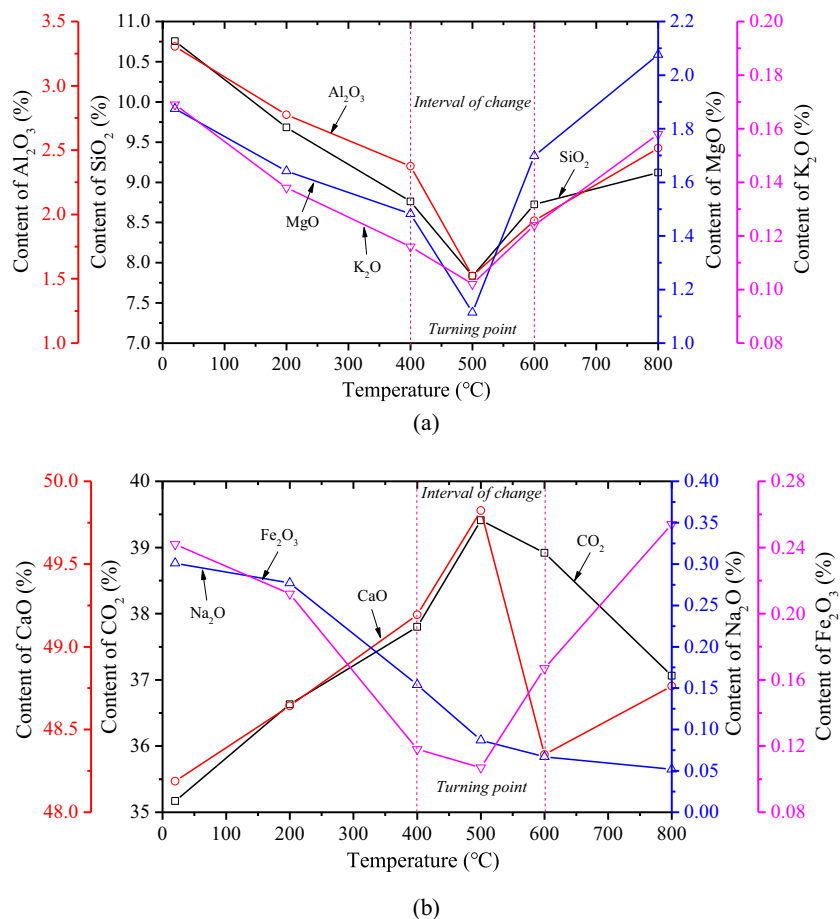
The data in the table is the average value of three rock specimens

500 °C, primary mineral components (illite) are gradually decomposed, dolomite is completely decomposed, and the diffraction intensity of calcite decreases significantly.

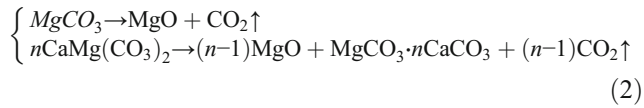
Al₂O₃, SiO₂, K₂O, and MgO contents are similar with the changing temperature (Table 3 and Fig. 4a). When $T \leq 400$ °C, the change in Al₂O₃, SiO₂, K₂O, and MgO contents is small; when $T = 400$ – 600 °C, Al₂O₃, SiO₂, K₂O, and MgO content is gradually reduced; and when $T = 600$ – 800 °C, Al₂O₃, SiO₂,

K₂O, and MgO contents increase rapidly. Na₂O content decreases slowly when $T \leq 200$ °C, while it decreases rapidly when $T > 200$ °C (Fig. 4b). CaO content increases rapidly when $T \leq 500$ °C, decreases rapidly when $T = 400$ – 600 °C, and increases again when $T > 600$ °C. Fe₂O₃ content decreases gradually when $T \leq 500$ °C and increases when $T > 500$ °C. CO₂ content increases gradually when $T \leq 500$ °C and decreases rapidly after 500 °C.

Based on XRD and XRF results, magnesite (MgCO₃), dolomite (CaMg (CO₃)₂), illite oxide (2SiO₂·Al₂O₃·2H₂O), ferrous hydroxide (Fe (OH)₂, Fe (OH)₃), calcium hydroxide (Ca (OH)₂), and infinitesimal minerals or impurities containing K₂O and Na₂O are the main elemental compositions altered when $T = 20$ – 800 °C. When $T \leq 200$ °C, the amount of infinitesimal minerals or impurities containing K₂O and Na₂O varies (the rapid decreasing curve of K₂O and Na₂O), as well as the decomposition of illite oxide (the decreasing curve of Al₂O₃ and SiO₂). When $T = 400$ – 600 °C, the decomposition of illite oxides, infinitesimal minerals or impurities containing K₂O and Na₂O, and calcium hydroxide occurs, resulting in gradual decreasing Al₂O₃, SiO₂, and K₂O curves as well as a rapidly increasing CaO curve. When $T = 600$ – 800 °C, the MgO curve rises rapidly, and the CO₂ curve decreases rapidly, corresponding to the decomposition of magnesite at 500–

Fig. 4 Variation of mineral content in limestone samples with temperature

600 °C and dolomite at 700–800 °C. Generally speaking, the CaO content changes little at different temperatures, indicating that calcite (CaCO_3) does not decompose below 800 °C.



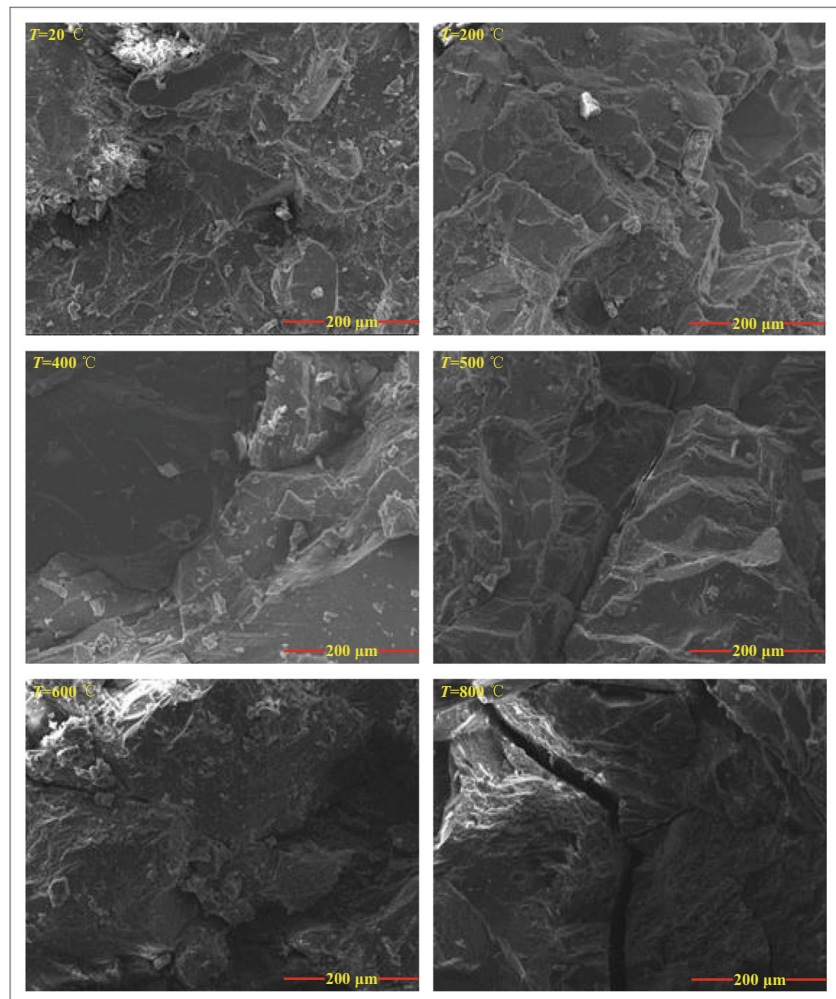
Analysis of micro-fracture morphology of limestone after high temperature

Rock micro-morphology analysis is an important method of examining rock micro-structure (Song et al. 2019; Guo et al. 2019). Rock fracture morphology is a record of the fracture process, reflecting the effect of temperature on the rock structure. A FEI Quanta™ 250 scanning electron microscope (SEM) is used to analyze fracture morphology (microstructure and defects) at different temperatures (magnification $\times 500$, Fig. 5). (1) When $T = 20$ °C (room temperature), fracture surfaces are relatively flat. Crystal particles are staggered with

different sizes, and there are large particles and micropores without obvious fractures. (2) When $T = 200$ – 500 °C, pits of different shapes are visible on the fracture surface. The amount of voids increases significantly, and micro-fractures characterized by intergranular fractures with rough edges begin to develop. Fractures are straight or curved, and vertical or oblique cross-layering is mainly characterized by tensile fracturing. (3) When $T = 600$ – 800 °C, the internal fabric and structure of rock sample tends to be weak. With the development of pores and fractures, micro-fractures converge into large pores. There are more slender fractures between particles and granule interiors, and most of them are linear, longer shear fractures and micropores, with few tensile fractures. Intergranular fractures and transgranular fractures exist simultaneously, and some crystal particles are damaged or destroyed, forming a network of connected fractures.

In general, fractures inside the limestone are generated and expanded with increasing temperature, and long fractures are finally formed after increasing the number and length of micro-fractures. At low temperatures, tensile fractures are dominant in the rock sample. When the temperature reaches 600–

Fig. 5 Fracture surface morphology for limestone samples at different temperatures ($\times 500$)



800 °C, shear fractures appear and increase gradually. At high temperatures, micro-fracture propagation and penetration are much more obvious than that at low temperature, resulting in decreased rock strength. Generally, the grain inside the rock varies at high temperature. After continuous accumulation, these grains dislocate each other, and the intergranular interface is destroyed. Then a secondary mesoscopic fracture forms around the intergranular interface. The existence, expansion, and convergence of a large number of micro-fractures eventually lead to macroscopic fracturing of rock samples. The effect of high temperature on micro-fracture morphology of limestone is mainly manifested in microvoids, intergranular cracks and transgranular cracks (Xu et al. 2008; Xu and Zhang 2016; Sun et al. 2016). With the increasing temperature, the original microvoids and micro-fractures in limestone gradually expand. Simultaneously, physical and chemical reactions, such as the dehydration, chemical bond fracture, and decomposition, result in the development of new holes and fractures. The influence of temperature on the crystal structure is manifested in the crystalline structure, as intergranular or transgranular cracks, and chemical bond breakage. When limestone is exposed to high temperature, intergranular or transgranular fractures can develop when the internal thermal stress reaches a certain amount. These fractures and voids are interconnected and form a seepage channel.

Limestone pore structure after high temperature exposure

Pores or fractures which have irregular geometry are distributed throughout the limestone samples at multiple scales. Rock is porous medium, whose pore size, volume, distribution, connectivity, and other structural characteristics have important effect on mechanical properties and engineering responses (Al-Harhi et al. 1999; Gruescu et al. 2007; Ugur et al. 2014; Zhang et al. 2015). A quantitative description of pore size distribution can be used to establish a correlation model between microscopic pore characteristics and macroscopic physical and mechanical properties. Presently, main methods for observing micropore characteristics include the capillary pressure curve methods (mercury intrusion method, centrifuge method, and gas adsorption method), image analysis methods (scanning electron microscopy, CT scanning method, and nuclear magnetic resonance method), and three-dimensional pore structure simulation methods (microscopic slice combination method, X-ray diffraction imaging, and image slice reconstruction) (Ju et al. 2008; Gao et al. 2013; Nie et al. 2015). Capillary pressure curve methods quantitatively determine the geometric characteristics of pores and tunnels by measuring the capillary pressure. Since Washburn used the mercury intrusion method to determine pore size and distribution, it has become an important method for measuring capillary pressure and obtaining the pore structure of rocks (Shin

et al. 2015). After exposure to high temperatures, changes in water phase, fractures, and mineral compositions inside the rock result in variations to the pore structure. In this paper, a 9310 micropore structure analyzer is used to carry out mercury intrusion testing on the limestone samples after exposure to high temperature. The relationship between accumulative mercury content and pressure at different temperatures is shown in Fig. 6.

In general, mercury more easily enter larger pores and has some difficulty entering smaller pores. The complete mercury intrusion test includes the mercury injection and mercury removal (Fig. 6). As capillary pressure increases, mercury is gradually injected into the limestone pores, and the mercury inflow curve increases nonlinearly. When the capillary pressure reaches the maximum working pressure of the instrument, capillary pressure is reduced, and the mercury removal process begins.

When $T \leq 200$ °C, the mercury intrusion curve increases with increasing capillary pressure, and the mercury evacuation curve varies slightly with decreasing capillary pressure (Fig. 6), and the intrusion curve is consistent with the evacuation curve. When the temperature is low, the temperature damage to the limestone is small, pores within the sample are small, and the amount of injected mercury is relatively small. When $T = 20$ °C, the volume of injected mercury in the sample is $V_i = 0.03802$ mL, the volume of mercury exiting from the rock sample is $V_e = 0.01657$ mL, and the volume difference is $\Delta V_{ie} = 0.02145$ mL. When $T = 200$ °C, $V_i = 0.04805$ mL, $V_e = 0.02480$ mL, and $\Delta V_{ie} = 0.02325$ mL. When $T = 400$ – 500 °C, the mercury intrusion curve for the limestone sample changes rapidly with increasing capillary pressure, and the evacuation curve changes rapidly with decreasing capillary pressure. The area between the intrusion curve and evacuation curve (the volume of mercury remaining in the sample) increases significantly, indicating that high temperature causes

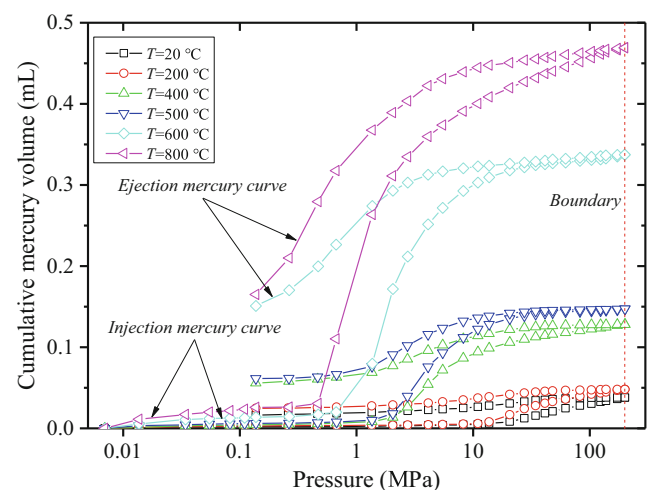


Fig. 6 Relationship between cumulative mercury inflow and pressure for limestone samples at different temperatures

significant damage to limestone when $T = 500$ °C, $V_i = 0.14724$ mL, $V_e = 0.06135$ mL, and $\Delta V_{ie} = 0.08589$ mL. When $T = 600$ – 800 °C, the limestone mercury intrusion curve (mercury withdrawal curve) changes sharply with increasing (decreasing) capillary pressure. Under high temperature, fractures in the limestone are continuously generated and expanded, resulting in increased porosity. The area formed between mercury intrusion curve and mercury evacuation is increases sharply, when $T = 800$ °C, $V_i = 0.46909$ mL, $V_e = 0.16496$ mL, and $V_{ie} = 0.30413$ mL.

The mercury intrusion method is based on a capillary bundle model, assuming that the porous medium is composed of bundles of pores with unequal diameters. Generally, without wetting the rock surface, mercury is a non-wetting phase; relatively speaking, the air or mercury vapor in the pores of the rock is the wetting phase. Injecting mercury into rock pores replaces the wetting phase with the non-wetting phase. When the injection pressure is higher than the capillary pressure corresponding to pore constriction, mercury enters the pore. At this time, the injection pressure is equivalent to the capillary pressure, the corresponding capillary radius is the pore constriction radius, and the volume of mercury entering the pore is the pore volume. The pore distribution curve and capillary pressure curve can be obtained by varying the injection pressure. The cumulative mercury intrusion curves of limestone samples at high temperatures show a step-wise non-linear increase, and the curves are divided into three stages: slow increase, fast increase, and slow increase (Fig. 7). Pore size ranges from 0.0036 to 105.79013 μm (Fig. 7). The maximum cumulative mercury intrusion from 20 to 800 °C increases from 0.03802 to 0.46909 mL, an increase of 12.33798 times. In addition, the slope of the curve indicates the volume of mercury entering the corresponding pore size, and the increasing temperature causes a change in shape of the curve. As the temperature increases, the number and size of pores inside the rock increases, the slope of the curve increases, and the amount of mercury in the rock sample increases significantly.

There is no universal standard method for classifying pore size. Considering the significance of pore size for gas and liquid adsorption and seepage, pore size can be divided into six types (Xu et al. 2008; Zhang et al. 2017): (1) ultramicro pores (less than 0.01 μm) which make up the adsorption volume; (2) micropores (0.01 – 0.1 μm), which make up the gas condensation and diffusion region; (3) small pores, (0.1 – 1.0 μm) which constitute the gas slow laminar permeability region; (4) mesopores (1.0 – 10.0 μm) which constitute the gas intense laminar permeability region where liquid can seep in at low permeability and higher pressure; (5) large pores (10.0 – 100.0 μm) which accommodate water seepage; (6) super large pores (> 100.0 μm) in which water can flow smoothly. According to the cumulative mercury intrusion curve in Fig. 7, the pore volume and its proportion under the corresponding

pore sizes can be obtained as shown in Table 4. Figure 8 shows the distribution ratio for the six pores types in limestone rock samples treated at different temperatures.

0.01 – 0.1 μm micropores before 200 °C account for about 71.47% , which decreases to 21.78% when a temperature of 500 °C is reached. The amount of micropores further decreased to 12.99% at 800 °C. Mesopores (1.0 – 10.0 μm) account for about 1.57 – 2.98% below 500 °C and account for 51.54% of the total pore space at 800 °C. The mesopore volume increased from 0.00439 to 0.24176cm^3 , an increase of 55.071 times when temperature increases from 500 to 800 °C. New fractures formed from increasing temperature are primarily mesopores. When $T = 500$ – 800 °C, pore structure characteristics changed significantly. The mesopore and large pore volume increases greatly, which leads to a significant increase in liquid permeability and a decrease in impermeability of the rock sample. After exposure to high temperature, micropores and small pores in the limestone samples are gradually transformed into mesopores, and the connectivity of fractures is enhanced.

Discussion

Effect of temperature on limestone porosity

Limestone porosity increases gradually with increasing temperature (Fig. 2). When $T \leq 200$ °C, porosity increases slowly with increasing temperature, which is only 1.338 times than that of the sample at room temperature (20 °C). When $T = 200$ – 500 °C, porosity increases rapidly with increasing temperature. When the temperature reaches 500 °C, the porosity is 1.351% , which is 3.871 times than that of the sample at room temperature (20 °C). When $T = 500$ – 800 °C, porosity increases sharply with increasing temperature. The porosity of the 800 °C sample reaches 3.899% , which is 11.172 times than that of the sample at room temperature (20 °C). Therefore, $T = 400$ – 500 °C can be regarded as a temperature threshold interval. When the heating temperature is lower than 400 °C, the porosity increase is slight. Above 400 °C, limestone samples undergo a dramatic porosity increase. In summary, rock samples undergo physical changes at a relatively low temperatures and chemical reactions at relatively high temperatures.

Limestone porosity variations with temperature can be divided into four stages: (1) When $T = 20$ – 100 °C, the attached water and interlayer water inside the rock escape in a short time because of their loose combination with minerals. This water is presented in tiny pores; thus, the change in porosity is small. (2) When $T = 200$ – 300 °C, the physically bound water inside the rock sample is lost in the form of water vapor. The high-pressure vapor escaping from the rock sample induces the generation and expansion of micro-fractures and

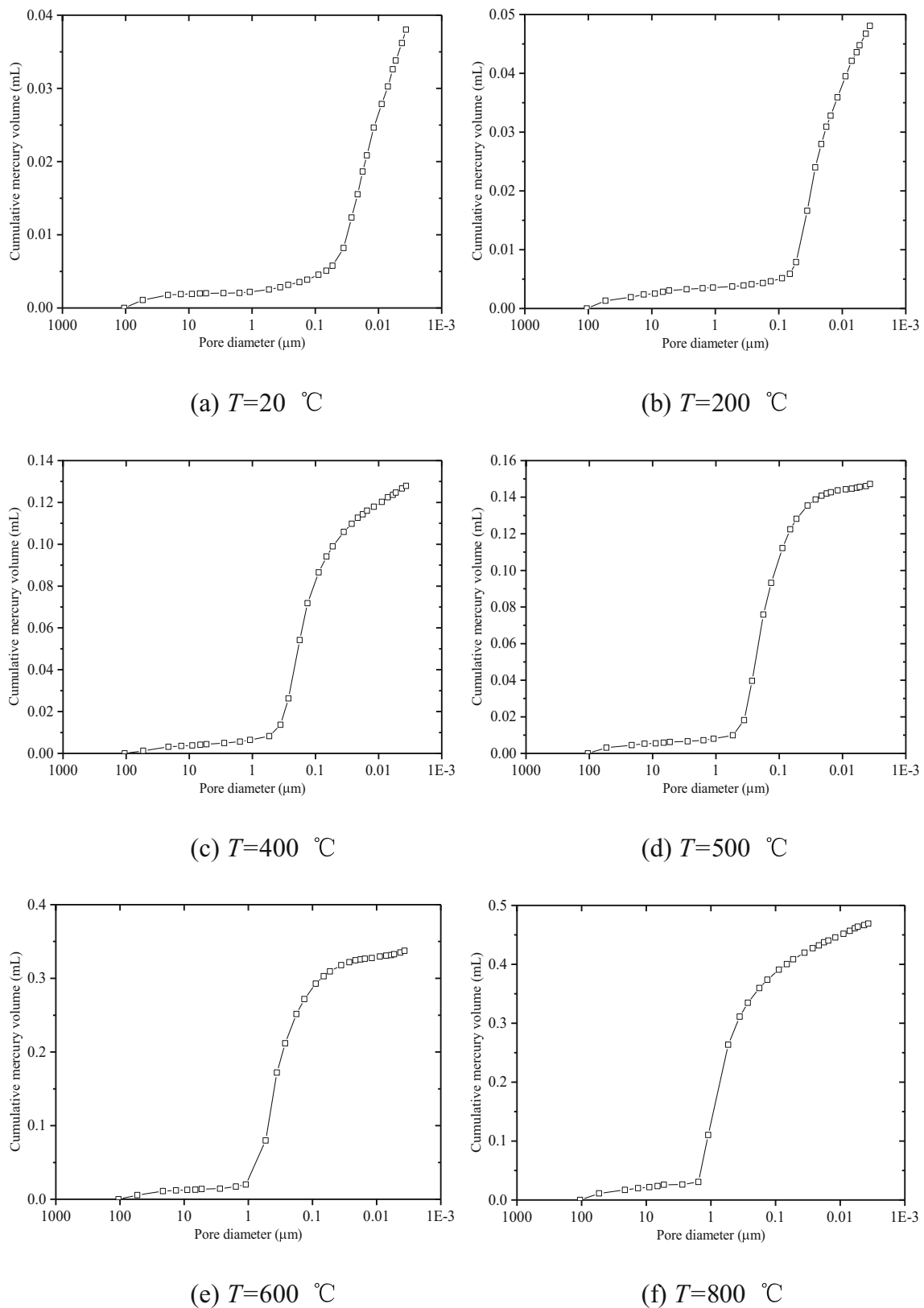


Fig. 7 Cumulative mercury intrusion curves for limestone samples at different temperatures

micropores, increasing porosity slightly. (3) When $T=300\text{--}500\text{ }^{\circ}\text{C}$, the attached water and physically bound water inside

the rock evaporate entirely. Chemically bound water, such as crystal water and mineral water, begin to precipitate, resulting

Table 4 Volume and proportion of pores with different sizes in limestone after high temperature exposure

Pore diameter (μm)	25 °C		200 °C		400 °C		500 °C		600 °C		800 °C	
	Volume (cm ³)	Ratio (%)	Volume (cm ³)	Ratio (%)	Volume (cm ³)	Ratio (%)	Volume (cm ³)	Ratio (%)	Volume (cm ³)	Ratio (%)	Volume (cm ³)	Ratio (%)
< 0.01	0.01016	25.69	0.00856	17.81	0.00762	5.96	0.00300	2.04	0.00777	2.30	0.01721	3.67
0.01~0.1	0.02331	61.32	0.03434	71.47	0.03369	26.34	0.03207	21.78	0.03691	10.94	0.06092	12.99
0.1~1.0	0.00204	5.36	0.00142	2.95	0.07837	61.28	0.10227	69.46	0.21300	63.08	0.12743	27.17
1.0~10.0	0.00060	1.57	0.00121	2.52	0.00437	3.42	0.00439	2.98	0.06717	19.91	0.24176	51.54
10.0~100.0	0.00084	2.20	0.00120	2.50	0.00263	2.06	0.00235	1.60	0.00686	2.03	0.01061	2.26
> 100.0	0.00107	3.85	0.00132	2.75	0.00120	0.94	0.00315	2.14	0.00573	1.74	0.01116	2.38

The data in the table is the average value of three rock specimens

in destruction of the mineral lattice. Mineral particles continue to expand, causing some cracks and pores to close, resulting in a less pronounced porosity increase. (4) When $T = 500\text{--}800\text{ }^\circ\text{C}$, the minerals in the limestone undergo a phase transition, metal bonds fracture, and some minerals melt, causing the number and volume of micropores to significantly increase. In addition to these physical and chemical reactions, with increasing temperature, thermal stress occurs within and between mineral particles due to mineral anisotropy and thermal expansion. When the strength criterion of mineral particles or particle contact surfaces is satisfied, new microfractures form and primary cracks continue to expand. The effective porosity of the rock is significantly increased by the primary isolated pores and closed pores in the connected sample. In summary, the change in limestone porosity under the influence of temperature is the combined result of physical effects (e.g., mineral dehydration), chemical effects (e.g., mineral phase transformation), and thermal cracking caused by uneven thermal expansion.

Rocks contain numerous micro-pores and micro-fractures. These micropores have different shapes in and distributions. A large number of experimental and theoretical studies have shown that materials show fractal characteristics at atomic and macro scales. Therefore, the micropores and micro-

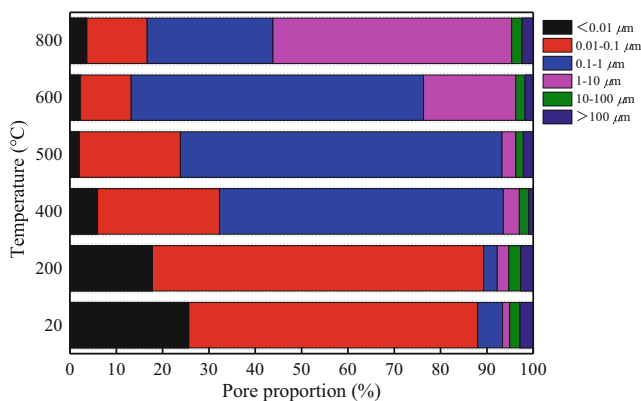


Fig. 8 Pore size distribution ratio for limestone samples at different temperatures

fractures can be regarded as a fractal network, and the pore distribution characteristics can be studied by using fractal theory (Qin et al. 2012; Chen et al. 2013; Zhao et al. 2015).

According to the fractal definition (Friesen and Mikula 1987; Xie and Gao 2000), $V(r)$ is proportional to r^{3-D_b} , and the pore volume is:

$$V_p(r) = V_0 - V(r) \quad (3)$$

where V_0 is the total volume of rock sample (including the solid medium volume and pore volume), cm³; V_p is the pore volume of rock sample, cm³; $V(r)$ is the rock volume measured using a volume element of size r ; D_b is the volume integral dimension; r is the pore size.

It can be obtained:

$$\lg(V_p/dr) \propto (2-D_b)\lg(r) \quad (4)$$

For pores in a cylindrical rock sample, the capillary pressure which is required for mercury to fill pores of size r is $p(r)$, and the relationship between $p(r)$ and r satisfies the Washburn equation:

$$p(r) = 2F \cos\theta / r \quad (5)$$

where the F is the mercury surface tension, N ; θ is mercury contact angle with the solid,

$$\lg(dV_p/dp) \propto (D_b-4)\lg(p) \quad (6)$$

where V_p is the volume of mercury injected into the pores.

In Eq. (6), $\ln(p)$ is the abscissa, and $\ln(dV_p/dp)$ is the ordinate. The slope k of the fitting line for $\ln(p)\text{--}\ln(dV_p/dp)$ can be obtained. The rock pore fractal dimension D_b is obtained, and the expression is $D_b = 4 - k$ (Zhang et al. 2017). The variation curve of the fractal dimension for limestone pores with temperature is obtained by calculation (Fig. 2).

Limestone pore fractal dimension varies slightly under the influence of temperature and is 3.076–3.190. When $T = 20\text{--}400\text{ }^\circ\text{C}$, the reduction is 1.88%; when $T = 400\text{--}500\text{ }^\circ\text{C}$, the reduction is 1.97%; when $T = 500\text{--}800\text{ }^\circ\text{C}$, the reduction is

3.73%. Limestone pore fractal dimension decreases gradually with increasing temperature. The original irregular fractures in the rock sample are gradually transformed into a uniform pore structure, which increases the porosity of the rock sample and the uniformity of the pore distribution, causing the gradual decrease of pore fractal dimension. $T=400\text{--}500\text{ }^{\circ}\text{C}$ can be used as the threshold value for variation in limestone pore fractal number.

Under high temperature, rock particles expand, causing a volume increase. Because of the volume change and thermal expansion anisotropy, the thermal stress manifests in the granule interior and between the rock particles. When heated to a certain temperature, the thermal stress inside the rock exceeds the strength criterion of the mineral particles or particle contact surface, and the internal structure of the rock is destroyed, resulting in new micro-fractures and changes in permeability and porosity. This temperature is called the rock thermal cracking threshold or threshold temperature. The threshold temperature of limestone is $400\text{--}500\text{ }^{\circ}\text{C}$, which is obtained from the physical and microstructure characteristics of limestone. Variations in pore characteristics with temperature can be explained based on the following two aspects.

(1) Pore structure and composition

Rocks are composed of different minerals, which contain attached water, bound water, and mineral bound water. The combination of attached water and bound water with minerals is relatively loose, and the water can be removed at $100\text{--}300\text{ }^{\circ}\text{C}$. While the temperature for removing crystalline water and mineral bound water in the crystal lattice is as high as $400\text{--}500\text{ }^{\circ}\text{C}$. Compared to the overall pore volume, the volume of the various water molecules in minerals should not be ignored. Below the threshold temperature, only the attached water and bound water are effected. These waters are located in tiny pores, so the permeability and porosity of the rock will change slightly. When the temperature is above the threshold temperature, physical and chemical reactions such as dehydration, decomposition, and phase transition occur, resulting in the rapid expansion of micro-fractures. The change in pore structure increases the fluid flow channel inside the rock, which in turn increases the porosity variation in the rock.

(2) Thermal stress under high temperature.

In addition to physical and chemical reactions, skeleton grains also expand and deform during heating, generating large thermal stress in the rock sample. The maximum thermal stress is concentrated on grain corners or the ends of micro-fractures. Solid particles have certain internal stress. When the thermal stress generated by heating exceeds the particle internal stress, the equilibrium state of the particles is destroyed, resulting in stress redistribution and a permeant change to the

rock internal structure. When the maximum thermal stress exceeds the yield strength of rock particles or cemented materials, micro-fractures are further expanded, or new cracks are generated at the contact points between particles. These new cracks destroy the original micro-fracture structure in the rock, increasing the connectivity of original fracture network. The flow capacity of the pores is improved, which increases the porosity of rock samples.

Studies have shown that threshold temperatures for thermal cracking of mineral components in different rocks are not the same, so the threshold temperature range is only statistically significant (Xu et al. 2008; Zhang et al. 2017). The thermal cracking of limestone is mainly related to the thermodynamic and mechanical properties of its mineral components. In addition to thermal expansion mismatch and thermal expansion anisotropy, mineral dehydration, lattice reorganization, mineral shrinkage, and decomposition during high temperature also increase fracture connectivity. In addition, the shape of the mineral particles also has a significant influence on thermal cracking, and the thermal cracking distribution is random.

Microscopic damage mechanism caused by temperature

As the temperature increases, the mineral volume inside the rock expands. Due to differences in thermal expansion coefficient and anisotropy, local thermal stress concentrations occur between mineral particles, causing microstructural mineral changes (Liu and Xu 2013; Rutqvist et al. 2002; Ranjith et al. 2012). The number of internal defects within the rock increases, and the physical and mechanical properties of the rock change at a macroscopic level. At the same time, the physical state of water inside the rock changes during the heating process, and the loss of constitution water and crystal water leads to the destruction of the mineral lattice. Under high temperature conditions, the number internal defects within the rock increases with moisture loss in some cases, resulting in a reduction of rock sample strength. Protodyakanov's Strength Index of rock (f), also known as the stability coefficient of rock, can be used to characterize the ability of a rock to resist damage. 1/10 of the uniaxial compressive strength of rock is generally regarded as the rock stability coefficient (Xiao et al. 2015). The relationship between the Protodyakanov's Strength Index of limestone and temperature is shown in Fig. 9 based on Eq. (7).

$$f = \frac{\sigma_c}{10} \quad (7)$$

where f is the rock Protodyakanov's Strength Index, and σ_c is the rock uniaxial compressive strength, MPa.

As shown in Fig. 2 and Fig. 9, (1) When $T \leq 200\text{ }^{\circ}\text{C}$, a small amount of minerals or impurities decompose, P -wave velocity decreases slowly, and there is no obvious physical

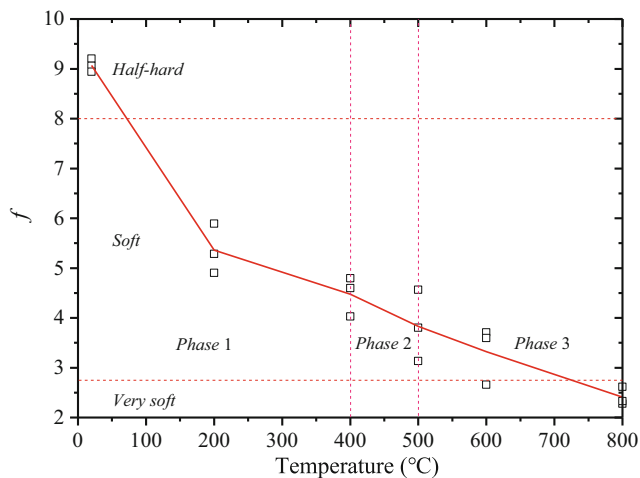


Fig. 9 Relationship between Protodyakanov's Strength Index and temperature

and chemical reaction. When the temperature rises from 20 to 200 °C, f decreases from 9.0677 to 5.36009, a reduction of 40.89%. The strength is greatly reduced. (2) When $T > 200$ °C, micro-fractures begin to develop and propagate gradually, the size and number of pores gradually increases, and pores become connected locally, resulting in a gradual increase in porosity and decrease in wave velocity. When $T = 400$ – 500 °C, the diffraction intensity of some calcite decreases, and minerals and calcium hydroxide decompose. The wave velocity and pore fractal dimension decrease slowly during this stage. In addition, f decreases 50.66% when $T = 400$ °C, and f decreases 57.73% when $T = 500$ °C. The above data indicate that $T = 400$ – 500 °C can be used as the threshold interval for phase transitions in limestone under high temperature. (3) When $T > 500$ °C, meilingite and dolomite decompose gradually. Pore size increases, and porosity increases significantly, while wave velocity decreases drastically. When $T = 800$ °C, f decreases to 2.40826, a reduction of 73.44%. The strength of limestone is greatly reduced. In general, as mineral phase transitions inside the rock progress, the internal structure changes rapidly, leading to increased porosity and decreased P -wave velocity. Macroscopically, the compressive strength of limestone is significantly reduced. During the mineral phase transition process, the energy inside the limestone is continuously changing. With the sudden increase of micro-fractures inside the rock sample, rock strength decreases sharply, and part of the energy accumulated in the rock sample is dissipated in the form of elastic energy, sound energy, and electromagnetic energy, which is reflected in the surge of acoustic emission signals and the increased electromagnetic radiation intensity (Glover et al. 1995; Zhang et al. 2017). Factors, such as mineral decomposition, crack growth, and chemical bond fracture, result in a nonlinear increase of porosity and a nonlinear decrease of limestone strength. The fractal dimension of limestone porosity decreases with

increasing temperature, indicating that the internal structure of limestone changes with increasing temperature.

Conclusion

In this paper, the evolution of limestone, P -wave velocity, mineral composition and content, micro-fracture morphology, and porosity with temperature are examined using physical and micro-structural tests on limestone exposed to high temperature. The following conclusions are drawn:

- (1) As temperature increases, limestone mass decreases and P -wave velocity decreases. When $T < 400$ °C, the reduction in mass and wave velocity is not significant. When $T = 400$ – 500 °C, the change of mass is significant, while the P -wave velocity decreases slowly. When $T = 500$ – 800 °C, the limestone mass loss rate increases sharply, and the P -wave velocity decreases dramatically. With increasing temperature, the attached water and mineral-bound water inside limestone are gradually lost. Mineral phase transitions, decomposition, and chemical bond fracture increase the limestone internal damage and porosity, leading to a decrease in mass and P -wave velocity.
- (2) When $T < 400$ °C, the change in chemical composition and crystal structure of limestone is not significant; when $T = 400$ – 500 °C, the diffraction intensity of partial calcite decreases, and dolomite decomposes gradually. When $T > 500$ °C, illite is significantly decomposed, dolomite is completely decomposed, and calcite diffraction intensity is significantly reduced. When $T \leq 200$ °C, the amount of infinitesimal minerals or impurities containing K_2O and Na_2O varies, as well as the decomposition of illite oxide. When $T = 400$ – 600 °C, illite oxide, trace minerals, or impurities containing K_2O and calcium hydroxide decompose. When $T = 600$ – 800 °C, magnesite and dolomite decompose. The change in CaO content is small at different temperatures, indicating that calcite ($CaCO_3$) does not decomposed at 800 °C. The decomposition and phase transition of minerals after exposure to high temperature leads to the development and expansion of micro-fractures and increased porosity, resulting in the deterioration of macroscopic limestone mechanical properties.
- (3) When $T = 20$ °C, fracture surfaces are relatively flat, and there is no significant crack development. When $T = 200$ – 500 °C, porosity increases, and micro-fractures begin to develop, most of which are intergranular fractures. When $T = 600$ – 800 °C, pores and fissures develop, and porous holes form between the particles. Intergranular cracks and the transgranular cracks exist simultaneously. With increasing temperature, original microvoids and micro-fractures in limestone are gradually expanded.

Physical and chemical reactions, such as the dehydration, chemical bonds fracture, and decomposition result in the development of new holes and fractures. The influence of temperature on minerals is mainly manifested in the crystalline structure, as intergranular or transgranular cracks and chemical bond breakage.

- (4) With increasing temperature, new fractures are 1.0–10.0 μm . Limestone porosity increases gradually with increasing temperature. When $T \leq 200$ $^{\circ}\text{C}$, porosity increases slowly with increasing temperature. When $T = 200$ – 500 $^{\circ}\text{C}$, porosity increases rapidly with increasing temperature. When $T = 500$ – 800 $^{\circ}\text{C}$, porosity increases sharply with increasing temperature. $T = 400$ – 500 $^{\circ}\text{C}$ can be used as a threshold interval for temperature. When the temperature is lower than $T = 400$ – 500 $^{\circ}\text{C}$, porosity increases slightly; when it is higher than this range, porosity increases significantly.
- (5) The pore distribution within limestone has fractal characteristics at various temperatures. The fractal dimension of pores is 3.076–3.195. With increasing temperature, fractal dimension decreases gradually, and the higher the temperature, the greater the decrease. Mineral dehydration, phase transition, and uneven thermal expansion induced by high temperature result in the breakage of mineral particles and expansion of native micro-fractures. Original irregular fractures are gradually transformed into a uniform pore structure, which increases the porosity and pore distribution uniformity of rock sample, causing a gradual decrease in pore fractal dimension. $T = 400$ – 500 $^{\circ}\text{C}$ can be used as the temperature threshold for the change in pore fractal number.

Funding information The financial and general supports for this research are provided by the National Natural Science Foundation of China (No. 51704280, 51809263), the Natural Science Foundation of Jiangsu Province of China (BK20160249), and the Fundamental Research Funds for the Central Universities (China University of Mining and Technology) (2015XKZD06).

References

- Al-Harathi AA, Al-Amri RM, Shehata WM (1999) The porosity and engineering properties of vesicular basalt in Saudi Arabia. *Eng Geol* 54(3–4):313–320
- Alm O, Jaktlund LL, Shaoquan K (1985) The influence of microcrack density on the elastic and fracture mechanical properties of Stripa granite. *Phys Earth Planet Inter* 40(3):161–179
- Brotóns V, Tomás R, Ivorra S, Alarcón JC (2013) Temperature influence on the physical and mechanical properties of a porous rock: San Julian's calcarenite. *Eng Geol* 167(4):117–127
- Chen YL, Ni J, Shao W, Azzam R (2012) Experimental study on the influence of temperature on the mechanical properties of granite under uniaxial compression and fatigue loading. *Int J Rock Mech Min* 56(15):62–66
- Chen J, Chen F, Xie N (2013) Study on fractal characteristics of pore structure in salt rock based on mercury injection data. *Disaster Adv* 6:12–19
- David C, Menéndez B, Darot M (1999) Influence of stress-induced and thermal cracking on physical properties and microstructure of La Peyratte granite. *Int J Rock Mech Min* 36(4):433–448
- Ersoy H, Kolayli H, Karahan M, Karahan HH, Sunnetci MO (2019) Effect of thermal damage on mineralogical and strength properties of basic volcanic rocks exposed to high temperatures. *B Eng Geol Environ* 78(3):1515–1525
- Ferrero AM, Marini P (2001) Experimental studies on the mechanical behaviour of two thermal cracked marbles. *Rock Mech Rock Eng* 34(1):57–66
- Friesen WI, Mikula RJ (1987) Fractal dimensions of coal particles. *J Colloid Interface Sci* 120(1):263–271
- Gao Z, Hu Q, Liang H (2013) Gas diffusivity in porous media: determination by mercury intrusion porosimetry and correlation to porosity and permeability. *J Porous Media* 16(7):607–617
- Glover PWJ, Baud P, Darot M, Meredith PG, Boon SA, LeRavalec M, Zoussi S, Reuschlé T (1995) α/β phase transition in quartz monitored using acoustic emissions. *Geophys J Int* 120(3):775–782
- Gruescu C, Giraud A, Homand F, Kondo D, Do DP (2007) Effective thermal conductivity of partially saturated porous rocks. *Int J Solids Struct* 44(3–4):811–833
- Guo JN, Liu JF, Li Q, Chen X, Chen ZQ, Huang BX, Chen SL (2019) Variation law of coal permeability under cyclic loading and unloading. *Therm Sci* 23(3b):1–8
- Hajpál M (2002) Changes in limestone of historical monuments exposed to fire or high temperature. *Fire Technol* 38(4):373–382
- Heap MJ, Baud P, Meredith PG (2009) Influence of temperature on brittle creep in sandstones. *Geophys Res Lett* 36(19):L19305
- Heard HC (1980) Thermal expansion and inferred permeability of climax quartz monzonite to 300 $^{\circ}\text{C}$ and 27.6 MPa. *Int J Rock Mech Min Sci Geomech Abstr* 17(5):289–296
- Heuze FE (1983) High-temperature mechanical, physical and thermal properties of granitic rocks - a review. *Int J Rock Mech Min Sci Geomech Abstr* 20(1):3–10
- Ju Y, Yang YM, Song ZD, Xu WJ (2008) A statistical model for porous structure of rocks. *Sci China Ser E* 51(11):2040–2058
- Just J, Kontny A (2012) Thermally induced alterations of minerals during measurements of the temperature dependence of magnetic susceptibility: a case study from the hydrothermally altered Soultz-sous-Forêts granite, France. *Int J Earth Sci* 101(3):819–839
- Kılıç Ö (2006) The influence of high temperatures on limestone P-wave velocity and Schmidt hammer strength. *Int J Rock Mech Min* 43(6):980–986
- Leiss B, Molli G (2003) 'High-temperature' texture in naturally deformed Carrara marble from the alpi apuane, Italy. *J Struct Geol* 25(4):649–658
- Liu S, Xu J (2013) Study on dynamic characteristics of marble under impact loading and high temperature. *Int J Rock Mech Min* 62(5):51–58
- Lo KY, Wai RSC (1982) Thermal expansion, diffusivity, and cracking of rock cores from Darlington, Ontario. *Can Geotech J* 19(2):154–166
- Lu YL, Wang LG, Sun XK, Wang J (2017) Experimental study of the influence of water and temperature on the mechanical behavior of mudstone and sandstone. *B Eng Geol Environ* 76(2):645–660
- Meng QB, Zhang MW, Han LJ, Pu H, Chen YL (2019) Experimental research on influence of loading rate on mechanical properties of limestone in high temperature state. *B Eng Geol Environ* 78(5):3479–3492
- Molen IVD (1981) The shift of the α - β transition temperature of quartz associated with the thermal expansion of granite at high pressure. *Tectonophysics* 73(4):323–342

- Nie BS, Liu XF, Yang LL, Meng JQ, Li XC (2015) Pore structure characterization of different rank coals using gas adsorption and scanning electron microscopy. *Fuel* 158:908–917
- Qin SG, Wu HL, Tian MB, Wu JC (2012) Fractal characteristics of the pore structure of low permeability sandstone. *Appl Mech Mater* 190-191:482–486
- Ranjith PG, Viete DR, Chen BJ, Perera MSA (2012) Transformation plasticity and the effect of temperature on the mechanical behavior of Hawkesbury sandstone at atmospheric pressure. *Eng Geol* 151:120–127
- Rocchi V, Sammonds PR, Kilburn CRJ (2004) Fracturing of etnean and vesuvian rocks at high temperatures and low pressures. *J Volcanol Geotherm Res* 132(2–3):137–157
- Rutqvist J, Wu YS, Tsang CF, Bodvarsson G (2002) A modeling approach for analysis of coupled multiphase fluid flow, heat transfer, and deformation in fractured porous rock. *Int J Rock Mech Min* 39(4):429–442
- Shin HS, Kim KY, Pande GN (2015) On computation of strain-dependent permeability of rocks and rock-like porous media. *Int J Numer Anal Methods Geomech* 39(8):821–832
- Song SB, Liu JF, Yang DS, Ni HY, Huang BX, Zhang K, Mao XB (2019) Pore structure characterization and permeability prediction of coal samples based on SEM images. *J Nat Gas Sci Eng* 67:160–171
- Su HJ, Jing HW, Mao XB, Zhao HH, Yin Q, Wang C (2015) Size effect of sandstone after high temperature under uniaxial compression. *J Cent South Univ* 22(5):1901–1908
- Su HJ, Jing HW, Yin Q, Yu LY, Wang YC, Wu XJ (2017) Strength and deformation behaviors of veined marble specimens after vacuum heat treatment under conventional triaxial compression. *Acta Mech Sinica* 33(5):86–898
- Sun Q, Zhang WQ, Xue L, Zhang Z, Su T (2015) Thermal damage pattern and thresholds of granite. *Environ Earth Sci* 74(3):2341–2349
- Sun Q, Zhang WQ, Su T, Zhu S (2016) Variation of wave velocity and porosity of sandstone after high temperature heating. *Acta Geophys* 64(3):633–648
- Tian H, Kempka T, Xu NX, Ziegler M (2012) Physical properties of sandstones after high temperature treatment. *Rock Mech Rock Eng* 45(6):1113–1117
- Ugur I, Sengun N, Demirdag S, Altindag R (2014) Analysis of the alterations in porosity features of some natural stones due to thermal effect. *Ultrasonics* 54(5):1332–1336
- Wu G, Wang Y, Swift G, Chen J (2013) Laboratory investigation of the effects of temperature on the mechanical properties of sandstone. *Geotech Geol Eng* 31(2):809–816
- Xiao SS, Li KM, Ding XH, Liu T (2015) Rock mass blastability classification using fuzzy pattern recognition and the combination weight method. *Math Probl Eng* 1:724619
- Xie HP, Gao F (2000) The mechanics of cracks and a statistical strength theory for rocks. *Int J Rock Mech Min* 37(3):477–488
- Xu XL, Gao F, Shen XM, Xie HP (2008) Mechanical characteristics and microcosmic mechanisms of granite under temperature loads. *J China Univ Min Technol* 18(3):413–417
- Xu XL, Zhang ZZ (2016) Fractal characteristics of rock fracture surface under triaxial compression after high temperature. *Adv Mater Sci Eng* 2016:2181438
- Yang SQ, Jing HW, Huang YH, Ranjith PG, Jiao YY (2014) Fracture mechanical behavior of red sandstone containing a single fissure and two parallel fissures after exposure to different high temperature treatments. *J Struct Geol* 69(Part A):245–264
- Yang SQ, Ranjith PG, Jing HW, Tian WL, Ju Y (2017) An experimental investigation on thermal damage and failure mechanical behavior of granite after exposure to different high temperature treatments. *Geothermics* 65:180–197
- Yavuz H, Demirdag S, Caran S (2010) Thermal effect on the physical properties of carbonate rocks. *Int J Rock Mech Min* 47(1):94–103
- Zhang WQ, Sun Q (2018) Identification of primary mineral elements and macroscopic parameters in thermal damage process of limestone with canonical correlation analysis. *Rock Mech Rock Eng* 51(4):1287–1292
- Zhang S, Paterson MS, Cox SF (2001a) Microcrack growth and healing in deformed calcite aggregates. *Tectonophysics* 335(1–2):17–36
- Zhang ZX, Yu J, Kou SQ, Lindqvist PA (2001b) Effects of high temperature on dynamic rock fracture. *Int J Rock Mech Min Sci* 38(2):211–225
- Zhang LY, Mao XB, Lu AH (2009) Experimental study on the mechanical properties of rocks at high temperature. *Sci China Technol Sci* 52(3):641–646
- Zhang LY, Mao XB, Liu RX, Li Y, Yin HG (2014) Meso-structure and fracture mechanism of mudstone at high temperature. *J China Univ Min Technol* 24(4):433–439
- Zhang ZT, Zhang R, Xie HP, Gao MZ (2015) The relationships among stress, effective porosity and permeability of coal considering the distribution of natural fractures: theoretical and experimental analyses. *Environ Earth Sci* 73(10):5997–6007
- Zhang YL, Sun Q, He H, Cao LW, Zhang WQ, Wang B (2017) Pore characteristics and mechanical properties of sandstone under the influence of temperature. *Appl Therm Eng* 113:537–543
- Zhao L, Wang W, Li Z, Chen YF (2015) Microstructure and pore fractal dimensions of recycled thermal insulation concrete. *Mater Test* 57(4):349–359